

Effects of stochastic growth and inter-filament correlation in an actin-inspired many-body Brownian ratchet

Evan Hohlfeld*

Lawrence Berkeley National Laboratory, Berkeley, California 94720

Phillip L. Geissler†

*Department of Chemistry, University of California, Berkeley,
and Lawrence Berkeley National Laboratory, Berkeley, California 94720*

We present a computational and theoretical study of a many-body Brownian ratchet, in which a “gel” of multiple, stiff polymerizing filaments pushes a diffusing obstacle. Our results show that steady-state dynamics of this system are strongly influenced by a layer of depleted filament density at the obstacle-gel interface. Inter-filament correlations within this molecule-thick layer have dramatic consequences for the velocity and structure of the growing gel. These emergent behaviors can be captured by mean field theories that emphasize the non-additivity of polymerization forces and indicate a key role for the fluctuating gap between gel and obstacle.

Living systems have evolved many processes that exploit fluctuations at the sub-cellular scale to transmute chemical energy into mechanical work. These processes, generally referred to as Brownian ratchets, propel cell motions such as crawling, phagocytosis, cytoplasmic streaming, organelle transport, and chromosome separation during anaphase [1]. Their essential physics is illustrated by a two-body model of a polymerization-based ratchet proposed by Peskin, Odell, and Oster [2]. Here, a single, stiff chain-molecule, such as an actin filament, pushes an obstacle with diffusion constant D , such as the cell membrane, microbead [3], or atomic force microscope cantilever [4], by polymerizing against it. Whenever a spontaneous fluctuation in the obstacle’s position opens a sufficiently large gap, a monomer of size a can stochastically intercalate and polymerize onto the filament at an average rate k_{on} . Because the filament is imagined to be anchored within a rigid gel, and because polymerization is taken to be irreversible, this stochastic event ratchets the obstacle’s diffusive advance, inducing a mean obstacle drift velocity v . The master equation for this *single*-filament model is exactly solvable for steady states at all values of D and external load f applied to the obstacle. In the limit $D \gg k_{on}a^2$ the resulting f - v relation has a simple form

$$v = ak_{on} \exp(-fa/k_{B}T), \quad (1)$$

where $k_{B}T$ is the available thermal energy [2].

The more biologically relevant problem of a *many*-filament ratchet is considerably less tractable, in part because inter-filament correlations make analytical treatment more difficult and in part because long relaxation times make computational study taxing. The single-filament model can be viewed as a caricature of such an N -filament system in which different filaments are assumed to polymerize and push independently, each bearing an effective load f/N [5, 6]. According to this approximation we could estimate the steady-state drift velocity v for an unloaded N -filament ratchet by setting

$f = f_{\text{drag}}/N = vk_{B}T/DN$, the portion of the drag force borne by each filament, in Eq. (1). We then obtain

$$v \approx 1 - \frac{1}{DN} \quad (2)$$

in the limit $DN \gg 1$. In Eq. (2) and below we adopt units of length and time such that $a = 1$ and $k_{on} = 1$.

The assumption that the pushing forces of filaments simply add has been used as a basis for many-body simulations [7], and to extract predictions for N based on f and v from phenomenological models in which N does not directly appear [8, 9]. It is also inherent to continuum models of growing gels [10, 11] wherein the polymerization force on an object results from the integral of a polymerization stress governed by a local constitutive law. All these approaches in effect assert that dynamics of the many-filament problem is well represented by growth of a single filament under an evenly distributed load; however, this assertion has never been verified for a *many*-filament model incorporating obstacle diffusion and stochastic polymerization with microscopic detail.

In this Letter we report on a set of simulation results and approximate theories of the N -filament ratchet that overcome previous difficulties, allowing scrutiny of the routinely neglected correlations among different filaments’ growth. We show that these correlations can in fact shape the steady-state velocity and internal structure of a many-body ratchet. In particular, our results highlight the significance of a microscopic layer of depleted filament tip density at the growing edge of the gel. Because of this depletion, apparently weak inter-filament correlations are amplified in their effect on structure and growth kinetics. This depleted layer has been discussed for related models [7, 12, 13], but its significance, nature, physical and mathematical origins, and generality for N -body ratchets were not explained.

The model we study, sketched in Fig. (1), is a generalization of the $N = 1$ ratchet [2] to the multi-filament

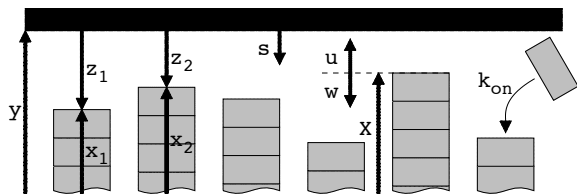


Figure 1: Monomers with height $a = 1$ (gray rectangles) stochastically polymerize at a mean rate $k_{on} = 1$ onto existing filaments with heights x_i , while the obstacle (thick black line) at y executes unbiased, one dimensional diffusion. Filaments are straight, parallel, rigid, and randomly aligned. The coordinate s and distances z_i are measured relative to y . Coordinates u and w are measured relative to $X \equiv \max_{i=1, \dots, N} x_i$.

case. Like that model ours lacks the chemical intricacies of any specific biological ratchet, instead focusing on generic physical features that are essential to its function. In detail, we consider N parallel, straight, rigid filaments (the “gel”) that push, via polymerization, against a diffusing obstacle with diffusion constant D and no external load. The position x_i of filament tip i advances stochastically in the $+x$ direction as a conditional Poisson process, taking discrete steps of size a with mean rate k_{on} so long as monomer addition would not penetrate the obstacle at position y . The obstacle in turn diffuses freely with a reflecting boundary condition at the leading edge of the gel, $X \equiv \max_i x_i$. We imagine that the base of each filament is firmly anchored (as in the $N = 1$ model), so that x_i increases in time on a fixed one-dimensional lattice. Because the actin gels we have in mind are highly disordered materials, we take the offsets among these lattices to be randomly distributed. The number of filaments N and the diffusion constant D are the only dimensionless parameters in our model. Biologically relevant values of D range from $D \approx 0.01$ for *L. monocytogenes* in cytoplasm [5] to $D \approx 10$ for patches of membrane [14]. We consider values of N between $N = 1$ and $N = 2^{14}$ ($= 16,384$).

We generated stochastic trajectories of our model using the continuous time Monte-Carlo method, which samples dynamics efficiently and exactly up to numerical round-off error. In our application of this method, time advances stochastically from the most recent attempted polymerization event at t to the next attempted event at $t + \tau$. The random waiting time τ between polymerization attempts is distributed as $p(\tau) = N \exp(-N\tau)$. At each attempt, a randomly selected filament polymerizes provided $x_i(t) + 1 < y(t + \tau)$. Between polymerization attempts, the obstacle moves diffusively with a reflecting boundary condition at $X(t)$. We initialized simulations by setting $y = a$ and randomly assigning $x_i(0)$ in the interval $[0, a]$, and then computed ensemble statistics by sampling configurations at uniform time intervals following establishment of a steady state. Approach to the steady state, however, becomes very slow as v approaches

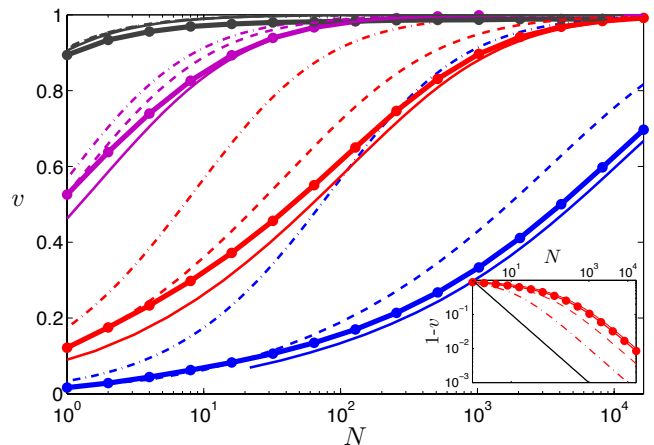


Figure 2: Dimensionless velocity, v , in steady state as a function of the number N of pushing filaments. Results are shown for simulations (points \bullet) with thick solid lines to guide the eye) and several predictions: based on additive polymerization forces (dash dotted line, by solving Eq. (1) with $f = v/DN$), from FMFT [Eq. (7)] (dashed lines), and from GMFT assuming $\alpha \equiv [\bar{\sigma}(1)/D]^{1/3} \gg 1$ [Eqs. (5) and (12-14)] (thin solid lines). Colors indicate different obstacle mobilities: $D = 10$ (black), 1 (magenta), 0.1 (red), and 0.01 (blue). (Inset) $1 - v(N)$ (colors and markers as in the main panel) compared with $1/N$ (solid black line).

one. To verify that our statistics are representative of terminal steady states, we confirmed that several exact conditions [detailed below in Eq. (4)] were satisfied.

Our key numerical results include $v(N, D)$ and the spatially resolved average density of filament tips. The small- N and large- N limits of $v(N, D)$ are dictated, respectively, by the Peskin-Odell-Oster solution for $N = 1$ and the average unobstructed polymerization velocity $v = 1$. Our simulation results presented in Fig. (2) show that the crossover between these limits is gradual, with $v \approx \log N$ over a large, intermediate range of N . For $N \gg 1$ we find that $v \approx 1 - \xi(D)/N$, where $\xi(D)$ is a dimensionless function of D . This asymptotic scaling with N is consistent with Eq. (2), though the prediction that $\xi(D) = D^{-1}$ is incorrect. Except for the largest value of D we consider, the number of pushing filaments required to sustain a given velocity is significantly underestimated by this heuristic prediction (by several orders of magnitude when $D \lesssim 1$ and $N \gg 1$).

As we show in Fig. (3a), for $N > 1$ the linear density of filament tips at distance s from the obstacle, $\rho(s)$, is marked by a monomer-thick layer of depleted filament density adjacent to the obstacle. Within mean field theories discussed below the many-body feature underlying this non-monotonic density profile is the steadiness of induced drift when multiple filaments are pushing. Polymerization stalls in $s < 1$, which for $N = 1$ transiently nullifies the effective force of ratcheting. For $N > 1$ stall of any one filament does not disrupt collective polymer-

ization forces, so that the flux of stalling filaments into $s < 1$ is balanced by obstacle drift (rather than by obstacle diffusion as for $N = 1$). This balance produces a microscopic zone of depleted tip density, which amplifies the influence of weak inter-filament correlations.

To clarify the relationship between steady state kinetics and microscopic structure at the gel's leading edge, we develop approximate analytical solutions to the master equation for the time-dependent configurational probability $P(y, x_1, \dots, x_N; t)$ of our N -filament model [15],

$$P_t = DP_{yy} + \sum_{i=1}^N \mathcal{T}_i P - P\Theta(y - x_i - 1) \quad (3)$$

[coordinate-name subscripts (i.e. t , y , s , and u) denote derivatives]. The first term on the right hand side of Eq. (3) represents free diffusion of the obstacle. The remaining terms, which involve the shift operator $\mathcal{T}_i f \equiv f(y, \dots, x_i - 1, \dots, x_N; t)$ and the Heaviside function $\Theta(x)$, represent stochastic growth of the filaments as constrained by the obstacle. Because obstacle diffusion is a continuous process, the mutual impenetrability of the obstacle and gel requires the boundary condition $P_y(\{y = x_i\}) = 0$ to prevent flux of probability to configurations that violate constraints of volume exclusion. For $N = 1$, Eq. (3) is identical to the equation studied in Ref. [2].

Steady-state solutions to Eq. (3) are most naturally described in a moving frame. Any coordinate that translates with average velocity v can serve as the origin of this frame. We will make use of two different choices, namely, the obstacle position y and lead filament position X . While the choice is physically immaterial, it determines which kinds of correlations can be treated straightforwardly when $N > 1$. Focusing first on the obstacle's motion, we define a set of relative coordinates $z_i \equiv y - x_i$. Because the lattice offsets are uniformly distributed, dependence of P on the z_i variables should be insensitive to the value of y at steady state.

We derive several exact relationships by evaluating moments of Eq. (3). In particular, at steady state the average y -current ($\int y P_t dx^N dy$) and average x_i -current ($\int x_i P_t dx^N dy$) both yield the mean drift velocity v . Integrating by parts, we can write these two moments in terms of average structural properties, specifically the filament tip density $\rho(s) \equiv \int_{\{z_i > 0\}} \sum_i \delta(s - z_i) P dz^N$ at a distance s from the obstacle, and the distribution $\psi(u) \equiv \int \delta(u - y + X) P dx^N dy$ of gap distance $u = y - X$:

$$v = D\rho(0) = D\psi(0) = \frac{1}{N} \int_1^\infty \rho(s) ds. \quad (4)$$

The last expression for v in Eqs. (4) was used in [2] for the $N = 1$ case; we primarily make use of the other two. According to the first relation, $v = D\rho(0)$, the effective force exerted on the obstacle, v/D , is proportional

to the average number of filaments *in contact* with it. The mechanical reasoning behind Eq. (2) does not acknowledge this sensitivity of polymerization forces to the gel's structure at contact, which is strongly shaped by multi-filament correlations.

We derive an equation for $\rho(s)$ from Eq. (3) by multiplying both sides by the density operator $\sum_i \delta(s - y + x_i)$ and integrating over x_1, \dots, x_N ,

$$D\rho_{ss} - D\rho_s^{(2)}(0, s) + \mathcal{T}_1 \rho - \rho\Theta(s - 1) = 0 \quad (5)$$

[16]. The corresponding boundary condition, $\rho_s(0) = \rho^{(2)}(0, 0)$, can be obtained in similar fashion. These results involve, but do not determine, the two-point correlation function $\rho^{(2)}(s, s') \equiv \int_{\{z_i > 0\}} \sum_{i \neq j} \delta(s - z_i) \delta(s' - z_j) P dz^N$. To close Eq. (5) we introduce a mean field approximation, which neglects correlated fluctuations in density at different positions s and s' ,

$$\bar{\rho}^{(2)}(s', s) \equiv \frac{N-1}{N} \bar{\rho}(s') \bar{\rho}(s) \quad (6)$$

[17]. This approximation, which we refer to as filament mean field theory (FMFT) and indicate with an overbar, is conceptually and mathematically distinct from the assumption of additive polymerization forces underlying Eq. (2). Substituting Eq. (6) into Eq. (5) yields a self-consistent equation

$$D\bar{\rho}_{ss} - D\bar{\mathcal{F}}\bar{\rho}_s(s) + \bar{\rho}(s+1) - \bar{\rho}\Theta(s-1) = 0, \quad (7)$$

where $\bar{\mathcal{F}} \equiv \frac{N-1}{N} \bar{\rho}(0)$. The corresponding boundary condition is $\bar{\rho}_s(0) = \bar{\mathcal{F}}\bar{\rho}(0)$. The solution of Eq. (7) is a piecewise linear combination of exponentials in s .

The nonlinear mean-field equation (7) is an effective one-body model for the many-body ratchet, which treats explicitly the stochastic growth of a single tagged filament and replaces the remaining $N - 1$ filaments with a constant effective driving force $\bar{\mathcal{F}}$. Its form is identical to the steady-state $N = 1$ master equation (3) for a system with an external load $\bar{\mathcal{F}}$, but with $\bar{\rho}$ replacing P and with the alternative normalization $\int_0^\infty \bar{\rho} ds = N$. FMFT determines the mean-field driving force $\bar{\mathcal{F}}$ self-consistently, requiring that it match the polymerization force \bar{v}/D emerging from the effective one-body problem on a per-filament basis, $\bar{\mathcal{F}}/(N - 1) = \bar{v}/DN$.

Predictions of FMFT for \bar{v} and $\bar{\rho}$, obtained numerically and shown in Figs. (2-3), improve upon the prediction heuristically derived from Eq. (1) over the entire range of N and D we have explored (greatly so for large N and small D). In particular, FMFT captures qualitatively the depletion of filament tip density at the gel's leading edge.

We can estimate $\bar{\rho}(s)$ asymptotically when $D \ll 1$ and $N \gg D^{-2}$ (so that $D\bar{\mathcal{F}} \sim \bar{v} \sim 1$, see below), shedding light on the depleted layer's origin. For $s > 1$, because obstacle drift nearly keeps pace with free polymerization,

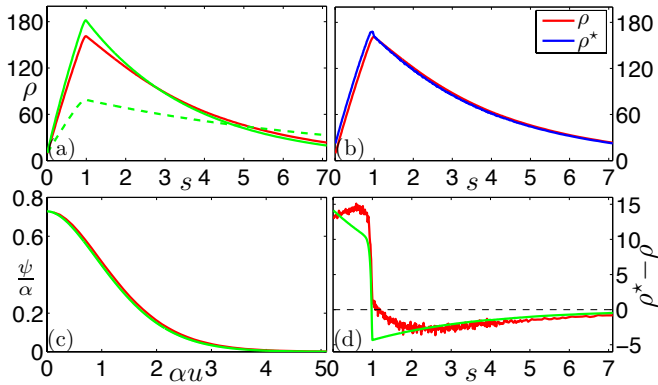


Figure 3: Steady state gel structure for $D = 0.1$ and $N = 600$, as determined from simulation and mean field theories. (a) Filament tip density $\rho(s)$, from simulation (red), from FMFT (dashed green line), and from GMFT (solid green line). (b) $\rho(s)$ (red line) and $\rho^*(s)$ [Eq. (8)] (blue line), both from simulation. (c) Gap distribution $\psi(u)$ from simulation (red) and from GMFT (green) (d) $\rho^*(s) - \rho(s)$ from simulation (red) and from GMFT (green). (a,c,d) For GMFT we assume $\alpha \gg 1$.

$\bar{\rho}$ varies slowly on the monomer scale $a = 1$. Using the gradient expansion $\bar{\rho}(s+1) \approx \bar{\rho}(s) + \bar{\rho}_s(s) + \frac{1}{2}\bar{\rho}_{ss}(s)$, we find that the mean drift of filament tips, $(1 - D\mathcal{F})\bar{\rho}_s$, is balanced by fluctuations in polymerization, $\frac{1}{2}\bar{\rho}_{ss}$, obtaining $\bar{\rho}(s) \sim \bar{\rho}(1)\exp[-2(1-\bar{v})(s-1)]$ for $s > 1$. From this form and the third of Eqs. (4) we also compute $\xi(D) = \frac{1}{2}\bar{\rho}(1)$. [In terms of $\bar{\rho}(1)$ and \bar{v} , these predictions of FMFT agree very well with simulation.] For $s < 1$, polymerization fluctuations are quenched, and the dominant balance of Eq. (7) is instead between obstacle drift, $D\mathcal{F}\bar{\rho}_s$, and the approximately constant influx of stalling filaments, $\bar{\rho}(s+1) \sim \bar{\rho}(1)$. This balance, the boundary condition for Eq. (7), and the first of Eqs. (4) immediately yield $\bar{\rho}(1) = D\mathcal{F}^2\bar{\rho}(0) \sim D^{-2}$, and predict $\bar{\rho}(s) \sim D^{-1} + sD^{-2}$ for $s < 1$. The actual solution to FMFT is smooth; here we neglect an exponential transition layer near $s = 1$ with width D . The general shape of $\bar{\rho}$ from FMFT agrees with simulation, but \bar{v} and $\bar{\rho}(1)$ differ significantly from simulation when $N \gg D^{-2} \gg 1$.

We checked the factorization hypothesis of FMFT, Eq. (6), using simulation data. Within FMFT the quantity

$$\rho^*(s) \equiv \frac{N}{N-1} \frac{\rho^{(2)}(0, s)}{\rho(s)} \quad (8)$$

should equal $\rho(s)$, and is indeed barely distinguishable from $\rho(s)$ except within the stall region $s < 1$ [see Fig. 3(b)]. Steady-state growth, however, is determined by the filament density precisely at contact, which is much lower than $\rho(1)$ for $N \gg 1$ due to the depleted layer. Relative to $\rho(0)$, deviations from Eq. (6) become in fact significant as $s \rightarrow 0$, leading to significant discrepancies between \bar{v} and simulation results.

One source of correlations neglected by FMFT is the

transient, *continuous* motion of the obstacle between *discrete* polymerization events. This motion uniformly shifts the instantaneous filament density profile as a function of the relative coordinate s . The resulting change in density at different values of s is highly correlated, involving all N filaments, and is difficult to capture in a theory based on the co-moving frame of the obstacle. Viewed relative to the lead filament, however, the gel's instantaneous density profile is insensitive to transient obstacle diffusion. This simple fact motivates a change of reference frame, in which the fluctuating variables include the gap u between gel and obstacle, and the lag $w_i = X - x_i$ of filament tips behind the lead filament.

Parallel to the development of FMFT, we compute from Eq. (3) an exact equation for the gap probability distribution $\psi(u)$,

$$D\psi_{uu} = \int_0^1 [\Pi(u, w)\Theta(w+u-1) - \Pi(u-w+1, w)] dw, \quad (9)$$

together with the boundary condition $\psi_u(0) = 0$. Solving Eq. (9) for $\psi(u)$ requires knowledge of the joint probability $\Pi(u, w) \equiv \int \sum_{j=1}^N \delta(u-y+X)\delta(w-X+x_j) P dx^N dy$ characterizing correlations between gap size u and filament density fluctuations at a distance w behind the lead filament. As before, we construct a closed set of equations through an approximate factorization,

$$\tilde{\Pi}(u, w) = \tilde{\psi}(u)\tilde{\sigma}(w), \quad (10)$$

here asserting statistical independence between fluctuations in gap size and those of the gel's internal structure. This alternative mean field hypothesis, which we call gap mean field theory (GMFT) and indicate with tildes, focuses attention on a distinct description of average gel structure, $\sigma(w) \equiv \int \sum_{j=1}^N \delta(w-X+x_j) P dx^N dy$, in which filament density is spatially resolved relative to the lead filament position.

Substituting Eq. (10) into Eq. (9) yields a self-consistent equation

$$D\tilde{\psi}_{uu} = \int_0^1 [\tilde{\psi}(u)\Theta(w+u-1) - \tilde{\psi}(u-w+1)] \tilde{\sigma}(w) dw \quad (11)$$

that requires as input the average filament density $\tilde{\sigma}(w)$. In our approach this input is obtained by solving the equations

$$\tilde{\rho}(s) = \int_0^\infty \tilde{\psi}(s-w)\tilde{\sigma}(w) dw \quad (12)$$

$$\tilde{\rho}^{(2)}(0, s) = \tilde{\psi}(0) \lim_{\epsilon \rightarrow 0^+} \tilde{\sigma}(s+\epsilon) \quad (13)$$

together with Eq. (5). Eqs. (12-13) follow from the exact relations

$$\rho(s) = \int_0^\infty \Pi(s-w, w) dw$$

$$\rho^{(2)}(0, s) = \lim_{\epsilon \rightarrow 0^+} \Pi(0, s)$$

using the factorization hypothesis Eq. (10).

GMFT, given by Eqs. (5) and (11-13), simplifies when the polymerization of filaments into the gap is fast compared to the diffusion of the obstacle over the distance $a = 1$. In this limit the average gap size, i.e., the width of the distribution $\tilde{\psi}(u)$, is much smaller than a ; the scale of variation of $\tilde{\sigma}(w)$, on the other hand, cannot be significantly smaller than a , due to the random offsets among different filaments' growth lattices. Treating $\tilde{\sigma}(w)$ as constant over the scale of decay of $\tilde{\psi}(u)$, we can reduce Eq. (11) to

$$\hat{\psi}_{\hat{u}\hat{u}} = \hat{u}\hat{\psi} - \int_{\hat{u}}^{\infty} \hat{\psi}(u')du', \quad (14)$$

where $\hat{u} \equiv \alpha u$, $\alpha \equiv [\tilde{\sigma}(1)/D]^{1/3} \gg 1$, and $\hat{\psi}(\hat{u}) = \tilde{\psi}(\hat{u}/\alpha)/\alpha$. For $\hat{u} \gg 1$, $\hat{\psi}(\hat{u}) \sim c \exp(-\hat{u}^{-3/2})$ for a constant c , in contrast to the exponential distribution of gap sizes for $N = 1$. The correspondingly more rapid decrease of $\tilde{\psi}$ with increasing u amounts to a renormalization of the diffusion constant D in the context of FMFT.

To determine the renormalized value of D , we first computed $\hat{\psi}(\hat{u})$ numerically from Eq. (14). Use of this result in Eqs. (12-13), Laplace transforms, and the separation in the scales of variation for $\tilde{\psi}$ and $\tilde{\sigma}$ yields the gradient expansion

$$\tilde{\rho}^{(2)}(0, s) = \tilde{\rho}(0)\tilde{\rho}(s) + \chi\tilde{\rho}_s + \dots, \quad (15)$$

where $\chi \equiv \hat{\psi}(0) \int_0^{\infty} u' \hat{\psi}(u') du' \approx 0.6844$. The first term in Eq. (15) differs from Eq. (6) of FMFT only in the absence of the pre-factor $(N-1)/N$. The second term in Eq. (15) is an $O(1)$ renormalization of D due to correlated density fluctuations neglected by FMFT. This renormalization alters the boundary condition for $\tilde{\rho}$ at $s = 0$, resulting in significant improvements to $\tilde{\rho}$ and \tilde{v} as compared to FMFT. Asymptotically for $N \gg D^{-2} \gg 1$, GMFT predicts $\tilde{\rho}(0) \sim D^{-1}$ and $\tilde{\rho}_s(0) \sim \tilde{\rho}(1)$, as in FMFT. It adjusts $\tilde{\rho}(1)$, however, $\tilde{\rho}(1) \sim (1-\chi)^{-1} D^{-2} \approx 3.17\tilde{\rho}(1)$ and yields $\xi(D) = \frac{1}{2}(1-\chi)^{-1} D^{-2} \approx 3.17\xi(D)$. We also find $\tilde{\sigma}(1) \sim \tilde{\rho}(1)$, and so $\alpha \sim (1-\chi)^{-1/3} D^{-1} \approx 1.47D^{-1}$ as $N \rightarrow \infty$ when $D \ll 1$. In Fig. (3d), we compare Eq. (15) with simulation. The solution to Eq. (14) agrees very well with simulations even for $\alpha \approx 10$ [see Fig. (3c)]. Eq. (13) also agrees well with simulation.

Note that like FMFT, GMFT is exact for $N = 1$. Of the two mean field theories, GMFT agrees more closely with simulations when $N \gg 1$. As such, GMFT is the natural starting point to analyze other physical effects in N -filament ratchet systems such the application of a load to the obstacle, filament and obstacle elasticity, Arp2/3

mediated filament-branching, three-dimensional gel ‘‘architecture’’, and adhesion between the obstacle and gel. Our results here suggest that many-filament ratchets are especially sensitive to physical effects that modify the dynamics of the fluctuating gap, but none of the aforementioned physical effects alter the applicability of the factorization hypothesis underlying GMFT. By separating the fast dynamics of the gap from the much slower chemical kinetics and elastic fluctuations of the gel, the structure of GMFT both correctly handles many-body correlations in growing gels and naturally lends itself to multi-scale simulation, which can overcome the problem of slow relaxation in more complex systems.

We thank Dan Fletcher for stimulating discussions. This work was supported by the U.S. Department of Energy, Office of Basic Energy Sciences, Division of Materials Sciences and Engineering, under Contract No. DE-ACO2-05CH11231.

* Electronic address: hohlfeld@berkeley.edu

† Electronic address: geissler@berkeley.edu

- [1] D. Bray, *Cell Movements: From molecules to motility, 2nd edition* (Garland Publishing, New York, 2001).
- [2] C. S. Peskin, G. M. Odell, and G. F. Oster, *Biophys. J.* **65**, 316 (1993).
- [3] L. A. Cameron, M. J. Footer, A. van Oudenaarden, and J. A. Theriot, *Proc. Natl Acad. Sci. USA* **96**, 4908 (1999).
- [4] S. H. Parekh, O. Chaudhuri, J. A. Theriot, and D. A. Fletcher, *Nature Cell Biol.* **7**, 1219 (2005).
- [5] A. Mogilner and G. Oster, *Biophys. J.* **71**, 3030 (1996).
- [6] A. Mogilner and G. Oster, *Biophys. J.* **84**, 1591 (2003).
- [7] T. E. Schaus and G. G. Borisy, *Biophys. J.*, **95**, 1393 (2008).
- [8] A. E. Carlsson, *Biophys. J.* **84**, 2907 (2003).
- [9] J. Weichsel and U. S. Schwarz, *Proc Natl Acad Sci USA* **107**, 6304 (2010).
- [10] J. Plastino and C. Sykes, *Curr. Opinon Cell Biol.* **17**, 62 (2005).
- [11] K. Sekimoto, J. Prost, F. Jülicher, H. Boukellal, and A. Bernheim-Grosswasser, *Eur. Phys. J. E* **13**, 247 (2004).
- [12] N. J. Burroughs and D. Marenduzzo, *Phys. Rev. Lett.* **98**, 238302 (2007).
- [13] K.-C. Lee and A. J. Liu, *Biophys. J.* **95**, 4529 (2008); **97**, 1295 (2009).
- [14] N. J. Burroughs and D. Marenduzzo, *J. Chem. Phys.*, **123**, 174908 (2005).
- [15] Note that P describes an *ensemble* of N -filament ratchets with *random* lattice alignment.
- [16] The shift operator \mathcal{T}_1 acts here on the only remaining coordinate, s , i.e., $\mathcal{T}_1\rho(s) = \rho(s+1)$.
- [17] The factor $(N-1)/N$ in Eq. (6) is required for proper normalization of $\tilde{\rho}(s)$ and $\tilde{\rho}^{(2)}(s, s')$.